

Quantum critical Mott transitions in a bilayer Kondo insulator-metal model system

Sudeshna Sen and N. S. Vidhyadhiraja*

Jawaharlal Nehru Centre for Advanced Scientific Research, Bangalore-560064, Karnataka, India

A bilayer system comprising a Kondo insulator coupled to a simple metal (KI-M) is considered. Employing the framework of dynamical mean field theory, the model system is shown to exhibit a surface of quantum critical points (QCPs), that separates a Kondo screened, Fermi liquid phase from a local moment, Mott insulating phase. The quantum critical nature of these Mott transitions is characterized by the vanishing of (a) the coherence scale on the Fermi liquid side, and (b) the Mott gap on the MI side. In contrast to the usual ‘large to small’ Fermi surface (FS) QCPs in heavy fermion systems, the bilayer KI-M system exhibits a complete FS destruction.

1. INTRODUCTION

The interaction driven Mott metal-insulator transition (MIT) is an integral aspect of a wide variety of phenomena exhibited by strongly correlated electron systems. The generic scenario for Mott MITs is that they are first order in nature, with a finite temperature critical end point¹⁻⁴, and are usually accompanied by large hysteresis curves, as seen for example in experiments on the vanadium oxides, V_2O_3 and VO_2 ^{5,6}. The two possible exceptions are (a) a bilayer ^3He system⁷, that can be pushed to a layer selective quantum critical Mott transition by tuning the filling of the layers⁸⁻¹³; and (b) two-dimensional organic insulators, where a pressure driven Mott quantum critical point (QCP) has been found very recently¹⁴.

The idea of a QCP in a Mott transition has thus far appeared as an exception rather than the rule, unlike in the case of heavy fermions that offer numerous examples of quantum criticality, which are driven either by spin or valence fluctuations^{15,16}. A recent work by Senthil¹⁷ proposed the possibility of observing a second order Mott transition from a Fermi liquid metal to a Mott insulator with a spinon Fermi surface in two dimensions. The role of critical fermionic quasiparticles has been proposed in the context of continuous Mott transitions and orbital selective Mott transitions at zero temperature^{15,17,18}. Recent study of quantum critical transport near the Mott transition in half-filled Hubbard model¹⁹ has been interpreted as evidence of a hidden Mott quantum criticality. Further study on doped Hubbard models reveal a clear connection between bad metal phenomenology and signatures of Mott quantum criticality²⁰. Studies of holographic duality propose the existence of yet-unspecified quantum critical regimes for strange metals in cuprates²¹. In order to obtain a better understanding of the continuous Mott MIT, it would be desirable to identify new systems where Mott quantum criticality may be observed.

In this paper, we consider a bilayer heavy fermion system comprising a Kondo insulator (KI), represented by a symmetric periodic Anderson model (PAM)^{1,22}, coupled to a non-interacting metal (M). Previous theoretical studies on coupling a KI layer to metallic layers have shown^{23,24} that the normally gapped f and c -bands of the KI acquire a finite density of states and a quadrati-

cally vanishing gap respectively due to the coupling. This emergent metallic phase of the f -electrons leads us to anticipate an interaction driven Mott transition. To our surprise, we find a plethora of interaction driven Mott QCPs in the KI-M system. The quantum critical nature of the Mott transitions is established by the vanishing of the coherence scale from the Fermi liquid side, and of the Mott gap from the insulating side at the same point in the parameter space. The competition between itinerancy and localization might lead to as yet unknown universality classes for the Mott transition²¹, and indeed, the system under consideration, might serve as an ideal model to investigate the universality and scaling associated with Mott quantum criticality.

2. MODEL, THEORETICAL FRAMEWORK AND ANALYTICAL RESULTS

The Hamiltonian of the bilayer KI-M model system is given by,

$$\begin{aligned} \mathcal{H} = & \sum_{\mathbf{k}i\sigma} \begin{pmatrix} f_{i\sigma}^\dagger & c_{\mathbf{k}\sigma}^\dagger & c_{M,\mathbf{k}\sigma}^\dagger \end{pmatrix} \begin{pmatrix} \epsilon_f & 0 & 0 \\ 0 & \epsilon_c + \epsilon_{\mathbf{k}} & 0 \\ 0 & 0 & \epsilon_{cM} + \epsilon_{\mathbf{k}} \end{pmatrix} \begin{pmatrix} f_{i\sigma} \\ c_{\mathbf{k}\sigma} \\ c_{M,\mathbf{k}\sigma} \end{pmatrix} \\ & + U \sum_i n_{fi\uparrow} n_{fi\downarrow} + V \sum_{i\sigma} \left(f_{i\sigma}^\dagger c_{i\sigma} + \text{H.c.} \right) \\ & + t_\perp \sum_{i\sigma} \left(c_{M,i\sigma}^\dagger c_{i\sigma} + \text{H.c.} \right) \end{aligned} \quad (1)$$

where ϵ_f is the orbital energy of the non-dispersive f -band, which is coupled to a conduction band with dispersion $\epsilon_{\mathbf{k}}$ and orbital energy ϵ_c through a hybridization V . These f - and c -orbitals belong to the KI layer, which is coupled to the metallic layer, characterised by a conduction band, $\epsilon_{\mathbf{k}}$, and an orbital energy, ϵ_{cM} , through an inter-layer hopping, t_\perp between the c -orbitals of the layers. The second term, represents the cost of double occupancy, U , of the f -orbitals of the KI layer.

In this work, we consider the particle-hole limit of this model where $\epsilon_c = \epsilon_{cM} = \epsilon_f + U/2 = 0$, and each of the three bands are half-filled. The KI-M model may be solved exactly in the non-interacting limit ($U = 0$), and the atomic limit ($V = 0$)²³. In order to investigate the

system beyond these simple limits, we employ the DMFT framework¹, within which the self-energy becomes local or momentum-independent. A cavity construction¹ for the bilayer model considered in Eq. (1) yields the following effective action for the f electrons:

$$S_{eff} = - \int_0^\beta d\tau \int_0^\beta d\tau' \sum_\sigma f_\sigma^*(\tau) \mathcal{G}_{0f}^{-1}(\tau - \tau') f_\sigma(\tau) + U \int_0^\beta d\tau n_{f\uparrow}(\tau) n_{f\downarrow}(\tau), \quad (2)$$

with,

$$\mathcal{G}_{0f}(\omega) = \int \frac{\rho_0(\epsilon)}{\omega^+ - \frac{V^2}{\omega^+ - \epsilon - t_\perp^2/(\omega^+ - \epsilon)}} d\epsilon \quad (3)$$

The f -Green's function may be written as $G^f(\omega) = \sum_k G^f(\omega, \epsilon_k) = \int_{-\infty}^{\infty} d\epsilon \rho_0(\epsilon) G^f(\omega, \epsilon)$, where, the $\rho_0(\epsilon) = 2\sqrt{1 - \epsilon^2/D^2}/(\pi D)$ is a semi-elliptic non-interacting conduction band density of states (DoS) of width $2D$, appropriate for a system with long-range hoppings, chosen to suppress magnetic ordering¹;

$$G^f(\omega, \epsilon) = \frac{\rho_0(\epsilon)}{\omega^+ - \frac{V^2}{\omega^+ - \epsilon - t_\perp^2/(\omega^+ - \epsilon)} - \Sigma_f(\omega)} \quad (4)$$

with $\Sigma_f(\omega)$ being the Hartree corrected, momentum-independent f -self-energy. Several results may be derived from these expressions, that are outlined below. For $U = V = 0$, the bilayer system undergoes a metal to band-insulator transition when the interlayer hopping exceeds the conduction band width. However, with $V \neq 0$, the non-interacting f -density of states, given by $D^f(\omega; U = 0) = -\text{Im}G^f(\omega; U = 0)/\pi$ does not vanish for any $t_\perp \neq 0$, although the $\omega = 0$ peak in the density of states gets progressively narrower with increasing t_\perp : $D^f(\omega; U = 0) \xrightarrow{t_\perp \gg 1} \frac{t_\perp^2}{V^2} \rho_0\left(\frac{\omega t_\perp^2}{V^2}\right)$. From the above expression, it is easy to see that, when $t_\perp \gg 1$, the effective bandwidth, D_{eff} of the f -DoS is greatly reduced as $\sim V^2/t_\perp^2$, hence the interaction strength needed for the Mott metal to insulator transition may be estimated as

$$U_c \sim D_{eff} \xrightarrow{t_\perp \gg 1} D V^2/t_\perp^2, \quad (5)$$

implying that the interaction strength required to drive the Mott transition should decrease rapidly with increasing inter-layer hopping.

The c -electrons in the heavy fermion layer acquire a self-energy, $\Sigma_{c1}(\omega)$ that can be related to $\Sigma_f(\omega)$ as, $\Sigma_{c1}(\omega) = \frac{V^2}{\omega^+ - \Sigma_f(\omega)}$. For, the non-interacting metallic layer, $V = 0$ and hence, $\Sigma_{c2}(\omega) = 0$. In our previous work²³ we had shown that for a bilayer system, the c -electron Greens functions are given by,

$$G_{11}(\omega) = a H[\Gamma_+] + b H[\Gamma_-], \quad (6)$$

$$G_{22}(\omega) = a' H[\Gamma_+] + b' H[\Gamma_-], \quad (7)$$

where

$$\Gamma_\pm = \frac{1}{2} \left(\lambda_1 + \lambda_2 \pm \sqrt{(\lambda_1 - \lambda_2)^2 + 4t_\perp^2} \right), \quad (8)$$

$$\lambda_r = \omega^+ - \epsilon_c - \Sigma_{cr}(\omega), \quad r = 1, 2$$

$$a = \frac{\Gamma_+ - \lambda_2}{\Gamma_+ - \Gamma_-} \quad \text{and} \quad b = \frac{\lambda_2 - \Gamma_-}{\Gamma_+ - \Gamma_-}, \quad (9)$$

$$a' = -\frac{\lambda_1 - \Gamma_+}{\Gamma_+ - \Gamma_-} \quad \text{and} \quad b' = \frac{\lambda_1 - \Gamma_-}{\Gamma_+ - \Gamma_-}, \quad (10)$$

and $H[z]$ represents the Hilbert transform with respect to the bare DoS of the conduction electrons. Using these expressions one may then derive a low energy form of the respective spectral function. In the low frequency regime of a Fermi liquid (FL) phase, where the f self-energy may be expanded in a Taylor series as: $\Sigma_f(\omega) = \Sigma_f(0) + \omega(1 - 1/Z) + \mathcal{O}(\omega^2)$ (where Z is the quasiparticle weight), the DoS of the c -e's of the heavy fermion layer has the following form:

$$D_1^c(\omega) \xrightarrow{\omega \rightarrow 0} \left(\frac{\omega t_\perp}{Z V^2} \right)^2 \rho_0 \left(\omega \left[1 + \frac{t_\perp^2}{Z V^2} \right] \right) + \left(1 - \left(\frac{\omega t_\perp}{Z V^2} \right)^2 \right) \rho_0 \left(\omega \left[1 - \frac{t_\perp^2}{Z V^2} \right] - \frac{Z V^2}{\omega} \right). \quad (11)$$

Further, since $D^f(\omega) = (Z^2 V^2/\omega^2) D_c(\omega)$, the f -e⁻ DoS at $\omega = 0$ is pinned to the non-interacting limit namely, $V^2 D^f(0)/t_\perp^2 = \rho_0(0)$, thus exhibiting adiabatic continuity to the non-interacting limit and hence satisfying a necessary condition for a Fermi liquid (FL). In a Mott insulating phase, on the other hand, the self-energy must have a pole at $\omega = 0$ with the form $\Sigma_f(\omega) \xrightarrow{\omega \rightarrow 0} \alpha/\omega^+$, where the residue of the pole is $\alpha \sim \mathcal{O}(U^2)^{1,25}$. So, if the bilayer system should have a Mott insulating phase, the denominator of $G^f(\omega; \epsilon)$ should not have zeroes for any $|\epsilon| < D$ as $\omega \rightarrow 0$, since that would imply a non-zero density of states in the single-particle spectrum at the chemical potential. It may be shown easily that such a condition is satisfied only for $t_\perp > D$. This condition can also be derived by substituting, $\Sigma_f(\omega) \xrightarrow{\omega \rightarrow 0} \alpha/\omega^+$, in Equation (7). Thus, a Mott insulating phase can be sustained only if $t_\perp > D$.

From the above analysis, we can anticipate a line of Mott transitions in the $t_\perp - U$ plane, where the critical U should decrease at least as rapidly as $1/t_\perp^2$ for $t_\perp \gg 1$ and for $U \rightarrow \infty$, the critical t_\perp should asymptotically approach the bandwidth D . In order to determine the phase diagram quantitatively, we must obtain the self-energy $\Sigma_f(\omega)$ and examine the quasiparticle weight as well as the Mott gaps. In this work, we choose the local moment approach (LMA) as the solver for the $T = 0$ quantum impurity problem. It is a diagrammatic perturbation theory based approach, which is built around the two broken-symmetry, local moment solutions ($\mu = \pm|\mu_0|$)

of an unrestricted Hartree-Fock mean field approximation. The spin-flip dynamics are subsequently incorporated through an infinite order resummation of a specific class of diagrams that represent the spin flip process necessary to capture the Kondo effect. Finally, a key ingredient of LMA is to impose adiabatic continuity to the noninteracting limit, that is crucial for the recovery of Fermi liquid behaviour and the emergence of a low energy scale. This is known as the symmetry restoration condition and any violation of this condition is a signal of a quantum phase transition to another phase such as a local moment phase. More details of the LMA may be found in previous work^{22,26}. The LMA has been shown to benchmark excellently against numerical renormalization group (NRG)²⁷, and Bethe Ansatz for the single impurity Anderson model and the Kondo problem respectively²⁶. Subsequently, it has been employed in studies on Kondo insulators and heavy fermion systems, where the dynamics and transport properties of several heavy fermions systems were quantitatively explained^{22,26,28}. The LMA has also been used in studying specific cases of impurity systems with many orbitals²⁹, the pseudogap Anderson model, the gapped Anderson impurity model and the soft-gap Anderson model^{30–32}. The study on the soft gap Anderson model has also been benchmarked with NRG³³. The resultant LMA phase boundary was in good quantitative agreement with NRG results³². However, generalizing LMA for employing it as a cluster solver to incorporate non-local dynamical correlations has not been attempted yet.

3. NUMERICAL RESULTS

3.1. Phase diagram

As discussed earlier, the LMA captures the Kondo effect through the calculation of the transverse spin-flip processes embodied in the infinite-order resummation of a specific class of diagrams²⁶. The low energy spin flip scale, ' ω_m ', thereby generated and identified through the position of the peak of the imaginary part of the transverse spin polarization propagator within LMA, is known to be proportional to the Kondo scale in the single impurity Anderson model²⁶. The ' ω_m ' scale is proportional to the quasiparticle weight ($Z = \left[1 - \frac{\partial \text{Re}\Sigma(\omega)}{\partial \omega}\right]^{-1}$) also, as shown in Fig. (1), where both Z and the ω_m are plotted and rescaled with simple multiplicative factors to highlight their equivalence.

Thus, we choose ω_m to be the coherence scale in the Fermi liquid phase. The vanishing of the ω_m scale then signifies the divergence of the effective mass at the Mott transition. In the Mott insulating phase, this low energy scale vanishes, i.e. $\omega_m = 0$ indicating a zero energy cost to flip an unscreened local moment and a Mott gap develops. The Mott gap then serves as the relevant energy scale in the Mott insulating phase. Conventionally, one

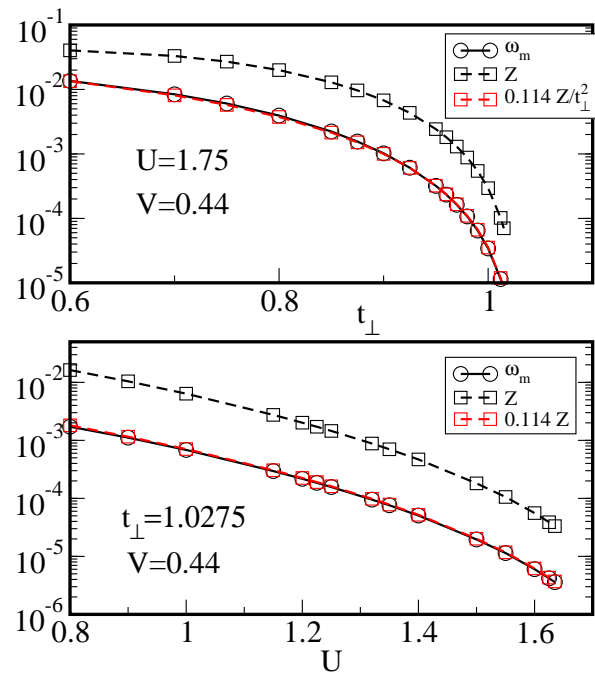


FIG. 1. **Comparison of the low energy spin flip scale, ω_m and the quasi-particle weight, Z :** ω_m (black circles) and the corresponding quasiparticle weight, Z (black squares), shown on the same scale. A simple multiplicative rescaling of the Z makes it identical to the ω_m data as shown by the red squares.

then probes the behaviour of these two relevant energy scales as a function of U to determine if there exists any regime of U where the metallic and the Mott insulating states may coexist, which would imply a first order Mott transition^{1,6,34–36}.

In Fig. (2) we therefore show the behavior of the FL scale ω_m , in the Kondo screened phase and the Mott gap, Δ_g in the Mott insulating state as a function of t_\perp (top panel) and as a function of U (bottom panel). Indeed, we find that the two scales vanish as power laws given by $\omega_m \sim (g_c - g)^{\alpha_{FL}}$ and $\Delta_g \sim (g - g_c)^{\alpha_{MI}}$, where the athermal parameter, g , represents t_\perp or U . It is seen from the top and bottom panels that either of the scales vanish at precisely the same (extrapolated) $t_{\perp c}$ (top) or U_c (bottom), thus indicating a quantum critical point in the $t_\perp - U$ plane.

A similar analysis for a wide range of values of U, V and t_\perp yields a family of lines of QCPs in the $t_\perp - U$ plane for various V values, as shown in Fig. 3(a). In Fig. 3(a) we show the line separating a Kondo screened phase from the Mott insulating phase, for different V 's, namely, $V = 0.44$ in the main panel and $V = 0.35, 0.5$ in the inset. These lines of QCPs represent a t_\perp driven Mott transition and the procedure adopted to obtain the $t_{\perp c}$ at a fixed U is demonstrated in Fig. 3(b, c). Additionally, we also demonstrate the line of QCPs corresponding to a U driven transition for $V = 0.5$ as represented as red squares in the inset of Fig. 3(a), found to be identical

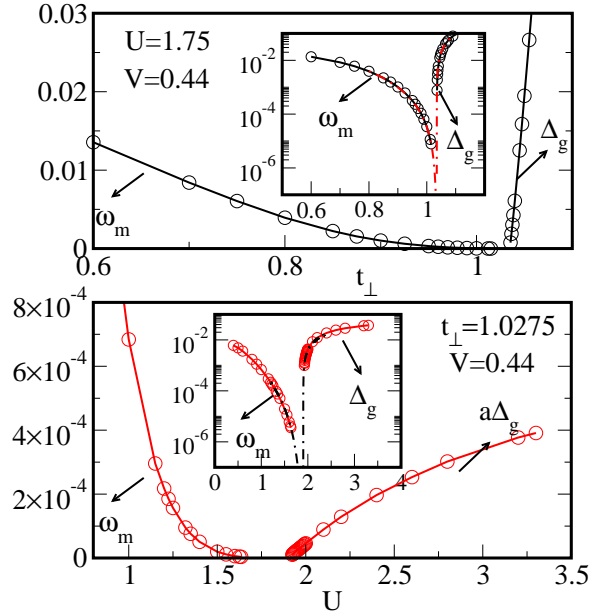


FIG. 2. The low energy spin flip scale, ω_m and the Mott gap, Δ_g for $V = 0.44$ as a function of t_\perp (top panel, $U = 1.75$, $t_{\perp c} \approx 1.03$) and U (bottom panel, $t_\perp = 1.0275$, $U_c \approx 1.9$). Note that in the main part of the bottom panel, the Mott gap values have been scaled by a multiplicative factor ($a = 1/95$) to show the ω_m and Δ_g on the same scale. In the insets, the same is plotted on a linear-log scale but the Mott gap is not rescaled. The extrapolation (dot-dashed line) to the critical value is shown to highlight that the Kondo scale and the Mott gap approach zero at the same critical point.

with the critical points obtained for a t_\perp driven transition. This confirms that U and t_\perp would drive the respective Mott MITs at the same critical point, irrespective of the direction of approach. In Fig. 3(a) (main panel), we find that while the curve *qualitatively* represent the analytical insight due to Eq. (5); however, the high t_\perp and low U asymptote appears to fit well with a form, $t_{\perp c} \sim f(V)/U_c^{0.2}$. While this quantitative discrepancy could stem from the approximate analytical argument, it could also be possible that we need to go to even lower U 's and even higher t_\perp 's to extract the form of the asymptote obtained from the numerical data.

We now mention the procedure adopted to extract the critical points in detail. For demonstration, we use the same data as shown in the top panel of Fig. (2). In the Fermi liquid phase (Fig. (3)(b)), the calculations were performed until a Kondo scale of $\sim 5 \times 10^{-5}$ was reached. Starting from an initial guess value, $t_{\perp c}^{guess}$ of the respective athermal variable, we then added/subtracted a small number ~ 0.001 from the simulated data points, plotted on a log-log scale. This subtraction/addition was then continued until a visually inspected straight line was obtained on the log-log scale and a fitting of the form $\omega_m = a|g - g_c|^{\alpha_{FL}}$ was done. The same was repeated for extrapolating the $t_{\perp c}$ while approaching the

MIT from the Mott insulating side. This is shown in Fig. (3)(c). As, shown in Fig. (3)(b) and Fig. (3)(c), ω_m and Δ_g vanish at the same critical point unlike a conventional Hubbard model at $T = 0$, indicating that the Mott MIT obtained in this model is a second order first transition. It is straightforward to see that each of these lines of QCPs is just a cut in the surface of QCPs in the $t_\perp - U - V$ space. This finding of an entire surface of Mott transitions, in a ‘new’ model, namely a bilayer KI-M model, that has not been explored before, represents the main result of this work. Moreover, our $T = 0$ calculations show that the Mott transitions are quantum critical in nature. The quantum critical surface separates two distinct phases, namely, a Kondo screened phase and a Mott insulating phase.

Our calculations show that the Mott quantum criticality that we discuss here involves a complete destruction of the Fermi surface (FS) in the f as well as c -spectrum (discussed in detail below) and is thus not a ‘large to small FS’ transition, in contrast to the generic QCPs observed in most heavy fermion systems¹⁶. Within DMFT, the electronic self energy is independent of momentum, and, hence the Mott critical points found here are local in nature. The possibility of a quantum critical Mott transition has been proposed earlier^{17,37}. Recent experiments¹⁴ on quasi-two dimensional organic systems suggest the existence of a $T = 0$ continuous Mott transition. Recent analyses of scaling behaviour of finite temperature resistivity curves in the half-filled¹⁹ and doped Hubbard model, computed through a continuous time quantum Monte Carlo solver within DMFT,²⁰ have been interpreted as evidence of hidden Mott quantum criticality. The current model of coupled symmetric PAM and noninteracting metal represents a new avenue where Mott quantum criticality can be studied in great detail within a microscopic Hamiltonian framework. Ideally one should analyse properties such as the specific heat and susceptibility in the proximity of a QCP and determine the critical exponents associated with them. Further the fixed points of the model should be found through renormalization group analysis in order to identify the universality class. We plan to carry out such analyses in future work.

3.2. Single-particle dynamics

A standard paradigm for investigating the Mott transition is the single band Hubbard model, where the first-order MIT (at $T = 0$) occurs by a continuous vanishing of Z at a critical interaction strength with the resonance pinned at $\omega = 0$ in the middle of a preformed gap^{1,34–36,38}. However, the Mott transition is not confined to just the Hubbard model but has also been observed in the symmetric PAM^{39,40} or other heavy fermion models, albeit with a dispersing f band⁴¹. The Mott transition in the symmetric PAM with nearest neighbour hybridization was justified⁴⁰ through the equiva-

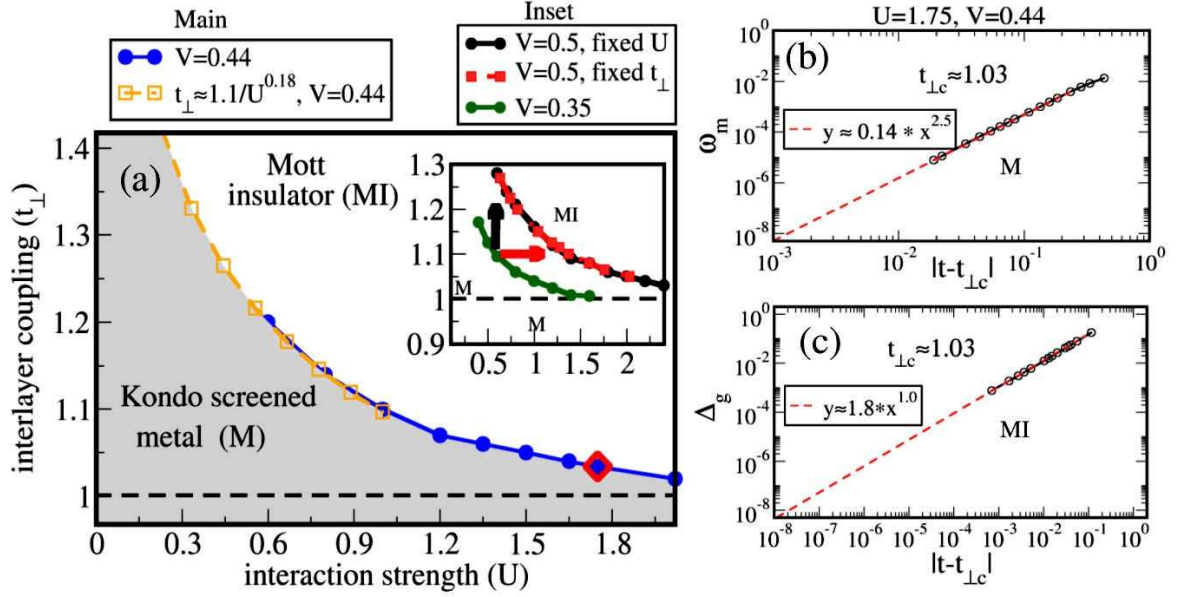


FIG. 3. The phase diagram in the $t_{\perp} - U$ plane for the transition from a Kondo screened Fermi liquid to a Mott insulating phase: (a) The main panel shows the line of QCPs obtained, for $V = 0.44$ (blue circles), and, the inset shows the same for $V = 0.5$ (black circles, red squares) and $V = 0.35$ (green circles). While for $t_{\perp} \gg 1$ it was estimated that $t_{\perp c} \sim \sqrt{DV^2/U_c}$, the numerical data, corresponding to low U asymptote, fits well to a form $t_{\perp c} \sim f(V)/U_c^{0.2}$ as represented by the orange dashed line with squares for $V = 0.44$ (also see main text). The black dashed line represents the $t_{\perp} = D$ boundary for the existence of the Mott transition. Additionally, in the inset, we also show, (for $V = 0.5$) that the line of quantum critical Mott transitions is the same irrespective of the direction of approach, namely, t_{\perp} driven (black circles, black arrow) or U driven (red squares, red arrow). (b, c) In order to identify the $t_{\perp c}$ or the U_c , we plot the ω_m (shown in (b) for $t_{\perp c}$) or the Δ_g (shown in (c) for $t_{\perp c}$) on a log-log scale. Starting from an initial guess value, $t_{\perp c}^{guess}$, we then add/subtract a small number ~ 0.001 from the simulated data points, plotted on a log-log scale. This subtraction/addition is continued until a visually inspected straight line was obtained that was fitted to the form $y = a|x - x_c|^{\alpha}$. The same procedure is repeated for U driven transitions. The representative plot corresponds to $U = 1.75, V = 0.44$ that also represents the top panel of Fig. (2). The corresponding extrapolated point is also highlighted as a red diamond in (a). The same is repeated for several other parameters and the phase diagram (a) in the $t_{\perp} - U$ plane is generated.

lence of the model to a single-band Hubbard model close to the Mott transition and at low frequencies ($\omega \sim ZD$). The bilayer KI-M model under consideration also has a similar equivalence, albeit with a difference. In a tiny neighbourhood of $\omega = 0$, the f -density of states has the form, $D^f(\omega) = (Z^2V^2/\omega^2)D_1^f(\omega)$. Thus, from (Equation (11)), it may be inferred that the current model is equivalent to a Hubbard model with a bare bandwidth of V^2/t_{\perp}^2 (from the first term) at the lowest frequencies ($|\omega| \ll ZD$); while for all other frequencies, the second term (gapped at the Fermi level) has a finite contribution. Moreover, it is clear that the first term is a function only of $\tilde{\omega} = \omega t_{\perp}^2/ZV^2$ while in the second term, a single scaling variable cannot be defined.

In Fig. (4) we plot the representative f -spectrum over all energy scales for different U 's and t_{\perp} 's in the FL phase (top panel) and the Mott insulating phase (bottom panel) at a fixed $V = 0.44$. In the Fermi liquid the structure on all scales is similar to that of the single band HM, namely that there are two Hubbard bands that move away from (towards) the Fermi level with increasing U (increasing t_{\perp}). In the Mott insulating phase at a fixed t_{\perp} (Fig. (4),

left bottom panel), in accordance with the conventional single band Hubbard model, Δ_g decreases with increasing U , simultaneously pushing the Hubbard bands out. However, with increasing t_{\perp} and a fixed U , the high energy Hubbard bands seem unaffected to a large extent (Fig. (4), right bottom panel).

We now look into the low energy sector of the correlated (f) and the conduction (c) electron spectrum of the heavy-fermion layer and the non-interacting metallic layer. Figure 5 shows the representative f -spectrum for the metallic case (top panels) and the insulating case (bottom panels) for a given QCP, reached either by increasing U (left panels) at a fixed $t_{\perp} = 1.0275$ or by increasing t_{\perp} at a fixed $U = 1.75$ for $V = 0.44$. The critical interaction strength for the left panels is $U_c \approx 1.9$ while the critical interlayer coupling for the right panels is $t_{\perp c} \approx 1.03$. The FL spectra, when scaled by V^2/t_{\perp}^2 , are seen to be universal functions of $\tilde{\omega} = \omega t_{\perp}^2/ZV^2$ in the scaling regime ($Z \rightarrow 0$ and finite $\tilde{\omega}$) as seen by the collapse of the spectra for a range of U or t_{\perp} values (left and right panels respectively). The insets in the two top panels show the same spectrum as the main panels, but on a

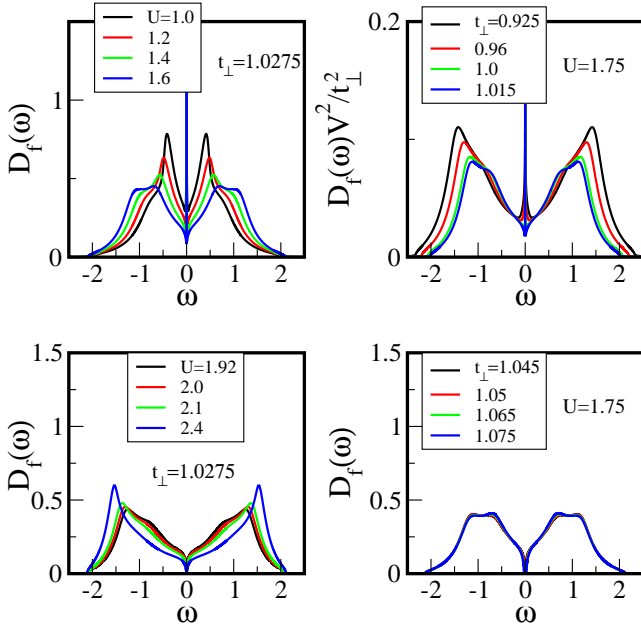


FIG. 4. The f electron spectrum across a U driven (left panels) and a t_{\perp} driven (right panels) QCP shown over all energy scales.

‘bare’ frequency scale that show the rapid narrowing of the central resonance peak upon approaching the QCP. The bottom panels show the Mott insulating spectra that show the single-particle gap to increase when the U or t_{\perp} is increased beyond the critical value. The insets in the bottom panel show that the Fermi surface is completely destroyed since the Mott gap in the f -DoS is identical to that in either of the conduction bands. Thus it is not orbital selective unlike the MIT observed in other related models^{40,41}.

We now show in Fig. (6) that, although the overall spectrum of the f electrons looks same as that of a single band HM, there lies a crucial difference: there is an absence of a preformed gap. It is now well known³⁶ that in the single band Hubbard model, the Kondo resonance in the metallic phase, resides inside a preformed insulating gap, such that at U_{c2} the resonance vanishes leaving behind a fully formed insulating Mott gap^{34,35}. In fact, this serves to be a spectral fingerprint of the first-order Mott transition observed in such systems^{1,6,34,35}. The absence of such a preformed gap in the metallic spectra of the f -electrons, as shown in Fig. (6) is crucially in agreement with the quantum critical nature of the Mott transition observed in the model. Here, the Hubbard band edges and the central Kondo resonance tails are connected by a finite density of states at all t_{\perp} ’s (Fig. (6))(left panel) and at all U ’s (Fig. (6))(right panel) sufficiently close to the transition, indicating that at the Mott transition, when the resonance vanishes, an insulating gap between the Hubbard bands just opens.

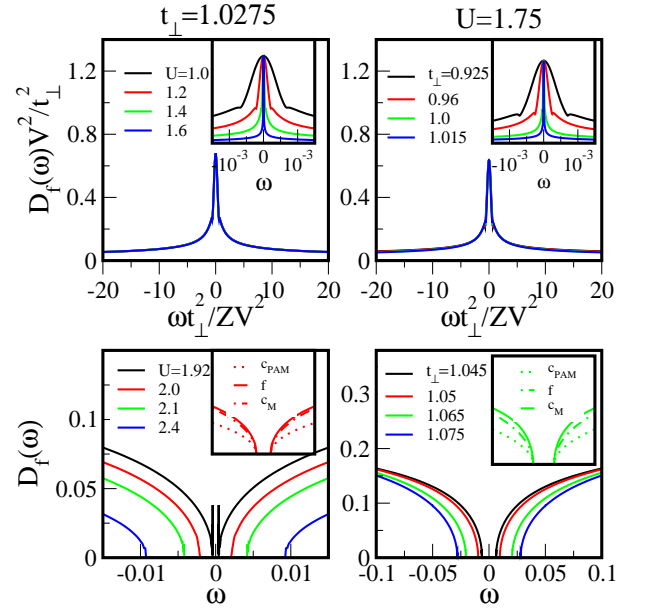


FIG. 5. f -spectrum across a U -driven (left panels) and a t_{\perp} driven (right panels) QCP. The top panels show the collapse of the Fermi liquid metallic spectra when plotted as a function of $\tilde{\omega} = \omega t_{\perp}^2 / ZV^2$, while the insets show the same spectra on a bare frequency scale. The bottom panels show the increase in the gap in the Mott insulating spectra with increasing U (left bottom) or increasing t_{\perp} (bottom right). The insets in the bottom panel show the c -spectrum of the heavy fermion layer (c_{PAM}) and the non-interacting metallic layer (c_M) on the same scale as the f -spectrum.

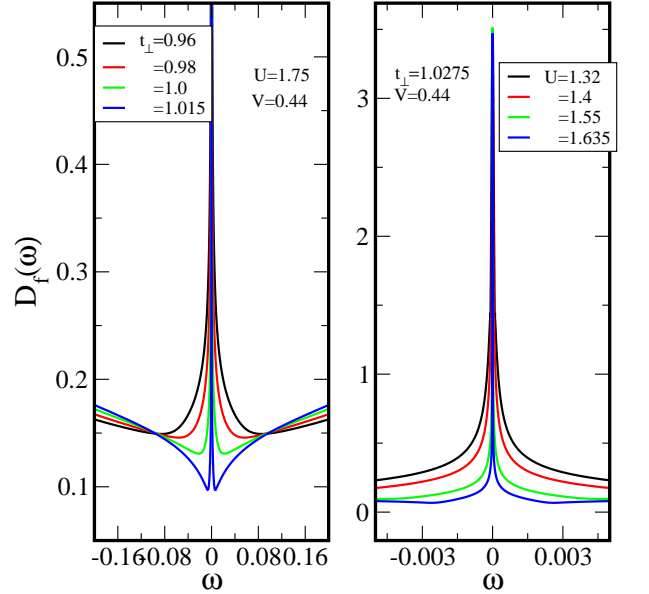


FIG. 6. The f electron spectrum across a U driven (left panels) and a t_{\perp} driven (right panels) QCP (close to the transition) shown over the low energy scales to highlight the absence of the formation of any preformed gap. The critical values are: $t_{\perp c} \approx 1.03$ in the left panel and $U_c \approx 1.9$ in the right panel.

4. CONCLUSIONS

We find a surface of Mott QCPs in a bilayer KI-M model, which may be accessed through three athermal parameters, namely the on-site Coulomb repulsion U , the interlayer-hopping t_{\perp} and the hybridization between f and c electrons, V . Experimental fabrication of precisely layered heavy fermion systems is indeed possible currently, and hence leads us to hope that the model proposed may be realized experimentally. In fact, we find that an M-KI-M system with the KI layer sandwiched between two non-interacting layers with interlayer hopping of $\sqrt{2}t_{\perp}$ is exactly equivalent to the bilayer KI-M model (equation 1), thus offering some more freedom in experimental fabrication. Additionally, we have checked that the use of a different c -electron DoS, such as a flat band or a two-dimensional tight-binding DoS with a van-Hove singularity at $\omega = 0$ does not change the scenario of a surface of QCPs qualitatively. Particularly, in the context of the current perspective, although a tuning of U and V is not straightforward, the t_{\perp} can be increased through uniaxial pressure, and hence the latter should be used as the experimental athermal parameter. Uniaxial pressure perpendicular to the planes could correspond to varying t_{\perp} , D and V simultaneously in a material-specific way. Theoretically, the equation of state, derived e.g. from a first-principles approach, might be able to yield the possible directions of approach that correspond to a single experimental variable. The structure of the model is not

limited to a Kondo-insulator-metal system but similar observations are expected to occur in any three orbital model that can be parametrized accordingly. However, the model Hamiltonian (equation 1) might not be a true representation of the real system, since many aspects of the latter such as f -orbital degeneracy, crystal field splitting, multiple conduction bands, and Hund's exchange, have been neglected. Moreover, for solving the model, we have neglected two-dimensional dynamical correlations (due to the use of the DMFT framework) and any symmetry breaking.

Nevertheless, the KI-M system could serve as a paradigmatic theoretical model, that brings together the phenomena of Mott transition, quantum criticality, and heavy fermions. Our work opens up a number of theoretical directions for exploration, such as the universality class and the relation of the QCPs found here to those found in impurity models⁴² such as the pseudogap Anderson model³⁰ or the gapped Anderson model³² as well as lattice models incorporating competition between Kondo screening and Ruderman-Kittel-Kasuya-Yosida interactions⁴³. Further investigations such as finite temperature critical scaling of transport and thermodynamic properties of the model are in progress.

ACKNOWLEDGMENTS

We acknowledge financial support from CSIR, India and JNCASR. We also acknowledge valuable discussions with M. Jarrell, R. C. Budhani, Subroto Mukerjee and Chandrabhas Narayana.

-
- * raja@jncasr.ac.in
- ¹ A. Georges, G. Kotliar, W. Krauth, and M. J. Rozenberg, *Rev. Mod. Phys.* **68**, 13 (1996).
 - ² G. Kotliar, E. Lange, and M. J. Rozenberg, *Phys. Rev. Lett.* **84**, 5180 (2000).
 - ³ H. Park, K. Haule, and G. Kotliar, *Phys. Rev. Lett.* **101**, 186403 (2008).
 - ⁴ E. Gull, P. Werner, X. Wang, M. Troyer, and A. J. Millis, *EPL (Europhysics Letters)* **84**, 37009 (2008).
 - ⁵ Z. Yang, C. Ko, and S. Ramanathan, *Ann. Rev. Mater. Res.* **41**, 337 (2011).
 - ⁶ P. Limelette, P. Wzietek, S. Florens, A. Georges, T. A. Costi, C. Pasquier, D. Jérôme, C. Mézière, and P. Batail, *Phys. Rev. Lett.* **91**, 016401 (2003).
 - ⁷ D. Vollhardt, *Rev. Mod. Phys.* **56**, 99 (1984).
 - ⁸ M. Neumann, J. Nyéki, B. Cowan, and J. Saunders, *Science* **317**, 1356 (2007).
 - ⁹ K. S. D. Beach and F. F. Assaad, *Phys. Rev. B* **83**, 045103 (2011).
 - ¹⁰ J. Werner and F. F. Assaad, *Phys. Rev. B* **90**, 205122 (2014).
 - ¹¹ A. Benlagra and C. Pépin, *Phys. Rev. Lett.* **100**, 176401 (2008).
 - ¹² A. Benlagra and C. Pépin, *Phys. Rev. B* **79**, 045112 (2009).
 - ¹³ A. Rançon Schweiger, A. Benlagra, and C. Pépin, *Phys. Rev. B* **83**, 073102 (2011).
 - ¹⁴ T. Furukawa, K. Miyagawa, H. Taniguchi, R. Kato, and K. Kanoda, *Nature Physics* **11**, 221 (2015).
 - ¹⁵ M. Vojta, *Journal of Low Temperature Physics* **161**, 203 (2010).
 - ¹⁶ Q. Si and F. Steglich, *Science* **329**, 1161 (2010).
 - ¹⁷ T. Senthil, *Phys. Rev. B* **78**, 045109 (2008).
 - ¹⁸ T. Senthil, M. Vojta, and S. Sachdev, *Phys. Rev. B* **69**, 035111 (2004).
 - ¹⁹ H. Terletska, J. Vučičević, D. Tanasković, and V. Dobrosavljević, *Phys. Rev. Lett.* **107**, 026401 (2011).
 - ²⁰ J. Vučičević, D. Tanasković, M. J. Rozenberg, and V. Dobrosavljević, *Phys. Rev. Lett.* **114**, 246402 (2015).
 - ²¹ S. Sachdev, *Phys. Rev. Lett.* **105**, 151602 (2010); R. A. Davison, K. Schalm, and J. Zaanen, *Phys. Rev. B* **89**, 245116 (2014).
 - ²² N. S. Vidhyadhiraja and D. E. Logan, *European Physical Journal B* **39**, 313 (2004).
 - ²³ S. Sen, J. Moreno, M. Jarrell, and N. S. Vidhyadhiraja, *Phys. Rev. B* **91**, 155146 (2015).
 - ²⁴ R. Peters, Y. Tada, and N. Kawakami, *Phys. Rev. B* **88**, 155134 (2013).
 - ²⁵ H. Barman and N. S. Vidhyadhiraja, *International Journal of Modern Physics B* **25**, 2461 (2011).
 - ²⁶ D. E. Logan, M. P. Eastwood, and M. A. Tusch, *Journal of Physics: Condensed Matter* **10**, 2673

- (1998); V. Smith, D. Logan, and H. Krishnamurthy, The European Physical Journal B **32**, 49 (2003).
- ²⁷ M. R. Galpin and D. E. Logan, Journal of Physics: Condensed Matter **17**, 6959 (2005).
- ²⁸ N. S. Vidhyadhiraja and D. E. Logan, Journal of Physics: Condensed Matter **17**, 2959 (2005).
- ²⁹ M. R. Galpin, A. B. Gilbert, and D. E. Logan, Journal of Physics: Condensed Matter **21**, 375602 (2009).
- ³⁰ M. T. Glossop and D. E. Logan, Journal of Physics: Condensed Matter **15**, 7519 (2003); EPL (Europhysics Letters) **61**, 810 (2003).
- ³¹ D. E. Logan and M. T. Glossop, Journal of Physics: Condensed Matter **12**, 985 (2000).
- ³² M. R. Galpin and D. E. Logan, The European Physical Journal B **62**, 129 (2008).
- ³³ R. Bulla, M. T. Glossop, D. E. Logan, and T. Pruschke, Journal of Physics: Condensed Matter **12**, 4899 (2000).
- ³⁴ M. J. Rozenberg, G. Kotliar, and X. Y. Zhang, Phys. Rev. B **49**, 10181 (1994).
- ³⁵ X. Y. Zhang, M. J. Rozenberg, and G. Kotliar, Phys. Rev. Lett. **70**, 1666 (1993).
- ³⁶ D. E. Logan and M. R. Galpin, Journal of Physics: Condensed Matter **28**, 025601 (2016).
- ³⁷ T. Misawa and M. Imada, Phys. Rev. B **75**, 115121 (2007).
- ³⁸ P. Nozières, Journal of the Physical Society of Japan **74**, 4 (2005).
- ³⁹ C. Huscroft, A. K. McMahan, and R. T. Scalettar, Phys. Rev. Lett. **82**, 2342 (1999); K. Held, C. Huscroft, R. T. Scalettar, and A. K. McMahan, Phys. Rev. Lett. **85**, 373 (2000).
- ⁴⁰ K. Held and R. Bulla, The European Physical Journal B **17**, 7 (2000).
- ⁴¹ C. Pépin, Phys. Rev. B **77**, 245129 (2008).
- ⁴² D. E. Logan, A. P. Tucker, and M. R. Galpin, Phys. Rev. B **90**, 075150 (2014).
- ⁴³ Q. Si, S. Rabello, K. Ingersent, and J. L. Smith, Nature **413**, 804 (2001).